

NONLINEAR DYNAMICS OF ATTRACTIVE MAGNETIC BEARINGS¹

K.V. Hebbale² and D.L. Taylor
Cornell University
Ithaca, New York 14853

The nonlinear dynamics of a ferromagnetic shaft suspended by the force of attraction of 1, 2, or 4 independent electromagnets is presented. Each model includes a state variable feedback controller which has been designed using the pole placement method. The constitutive relationships for the magnets are derived analytically from magnetic circuit theory, and the effects of induced eddy currents due to the rotation of the journal are included using Maxwell's field relations.

A rotor suspended by four electro-magnets with closed loop feedback is shown to have nine equilibrium points within the bearing clearance space. As the rotor spin speed increases, the system is shown to pass through a Hopf bifurcation (a flutter instability). Using center manifold theory, this bifurcation can be shown to be of the subcritical type, indicating an unstable limit cycle below the critical speed. The bearing is very sensitive to initial conditions, and the equilibrium position is easily upset by transient excitation. The results are confirmed by numerical simulation.

INTRODUCTION

The suspension of a rotating shaft in a magnetic field without mechanical contact or lubrication is an old idea. Many studies concerning the feasibility of electromagnetic levitation in various applications like magnetic bearings, high speed ground transportation, electromagnetic dampers for vibration control, etc. can be found in the literature [refs. 1,2,3]. Now, with advanced electronic control, high speed magnetic bearings are a commercial reality, being used in grinding and polishing machinery, vacuum pumps, compressors, turbines, generators, and centrifuges [refs. 4,5]. Electromagnetic dampers have been shown to be capable of effectively eliminating vibration at the critical speed associated with the first bending mode of shafts [refs. 3,6]. In addition, the dampers have been seen to suppress the system instability associated with the fluid film bearings.

This paper only considers attraction systems under active control. Passive systems using permanent magnets in repulsion are usually incapable of generating sufficient load carrying capacities. However, the constitutive model presented here is applicable to electromagnets operating at sufficient speed that the dead weight is carried by eddy currents generating lift from the lower magnet.

The control system studied varies the voltage to each magnet in response to the motion of the mass. Such a suspension system with multiple magnets is a multiple input - multiple output system. A state variable feedback controller, designed on the basis of pole placement technique, is used to stabilize the system and meet the design specifications. Unlike in a single input - single output system, the multivariable problem has a much richer structure and has many gain matrices yielding the same pole placement [ref. 7]. The direct method of choosing an arbitrary vector and reducing the multi-input - multi - output system into a single input - single output system is used to obtain the gain matrix.

Research and development activity on passive, active, and combination magnetic bearing systems spans over

¹This work was supported in part by the Office of Naval Research under contract no. N0014-80-C-0618.

²Presently at General Motors Research Laboratories.

150 years. Earnshaw in 1839 demonstrated [ref. 8] mathematically that it is impossible for a pole placed in a static field of force to have a stable equilibrium position when an inverse square law relates force and distance. Braunbek in 1939 carried out [ref. 8] a similar mathematical analysis specifically for suspensions in unvarying magnetic fields and deduced that levitation is impossible in such fields when all the materials have relative permeabilities (μ_r) greater than or equal to 1, but possible if materials with $\mu_r < 1$ can be introduced. It follows that it is impossible to achieve levitation in static magnetic fields, that is, using permanent magnets or fixed current dc electromagnets, unless part of the system consists of either diamagnetic material ($\mu_r < 1$) or a superconductor ($\mu = 0$).

Examples of hybrid passive and active systems appeared as early as 1950 in which photoelectric positional feedback was used. Stiffness and damping were minimal because of the lack of sophisticated control components. Early experiments with fully active systems (1957) were largely thwarted by the then high cost and size of control system components. In time, it became clear that hybrid systems with simple electronics capable of carrying industrial loads depended heavily on complex mechanical dampers. Meanwhile the cost and size of sophisticated electronics for purely active systems continued to come down as performance rose. Since active magnetic bearings provide both damping and support, the choice became clear. Subsequent efforts have concentrated on active magnetic bearings.

Several reviews of electromagnetic levitation are available in the literature [ref. 8,9]. Two electromagnetic levitation methods have met with success: direct, position feedback control techniques; and ac modulated or indirect feedback methods. In the latter, the magnet inductance is part of a tuned circuit whose natural frequency depends on the gap between the suspended mass and magnet. This method has been used to suspend gyroscopic devices for inertial sensors. It suffers from high eddy current losses and a small range of stable air gaps. Analysis of ac tuned circuit methods may be found in Kaplan [ref. 10].

For heavily loaded bearings, direct feedback methods have to be used. However, dynamics has not seen as much attention as it has in journal bearings. Most of the available literature deals with empirical ideas and concentrates on reliability of the bearing, reducing the size, weight and complexity of the devices [ref. 11].

Insight can be gained by studying a ferromagnetic suspension (suspended mass is not moving). Moon [ref. 12] and Woodson and Melcher [ref. 13] are good starting points.

When the suspended rotor is spinning under the magnets and if the rotor is not laminated, eddy currents will be induced in the material. The induced eddy currents create two kinds of force on the rotor: drag force which leads to additional power dissipation and coupling of motions of the rotor in two perpendicular directions, and repulsive force which tends to counter balance the attractive force. Expressions for the drag and repulsive forces can be derived by studying the effect of material motion on the diffusion of magnetic fields [ref. 13], starting from Maxwell's field relations. Moon [ref. 12] has shown that in certain magnetic levitation configurations eddy currents can produce a positive or negative damping force depending on the speed.

Although a good analytical model is not available for eddy currents due to shaft rotation, a number of authors calculate the eddy current effects in other geometrical configurations using a hypothetical simplified model and finite element methods [refs. 14,15]. Several studies on linear induction motors are available [refs. 1,16] which can be extended to magnetic bearings by making several assumptions and manipulations. In the above studies, the authors calculate the induced forces by cross multiplying the current density vector, which does not take care of the attractive force when the moving material is ferromagnetic. In this paper, the forces are calculated using the Maxwell's stress tensor approach which in one calculation gives all the forces involved.

Matsumara [ref. 17] has derived the fundamental equations for a horizontal shaft magnetic bearing taking into account the rolling, pitching, and yawing of the rotor. In deriving the equations of motion, he assumes that the rotor consists of a laminated core and consequently no eddy currents are generated in the material. He has proposed an integral type control system which stabilizes the system without steady state shaft position error.

Hebbale [ref. 18] has studied the nonlinear dynamics in terms of equilibrium points, transient response, on-set of instability, limit cycle size, and forced response. The material which follows was taken from [ref. 18].

NOMENCLATURE

| | |
|-------|--|
| a | Distance of magnet pole corner (near) from center line |
| A | Area of magnet pole face, Linearized state matrix |
| b | Distance of magnet pole corner (far) from center line |
| B | Control input matrix, a Magnetic Flux density |
| B_0 | Magnetic flux density under the magnet pole |
| C_i | Feedback gains of controller |
| D | Diameter of rotor |

| | |
|--------------|--|
| \vec{e} | Unit vectors |
| $E(t)$ | Control voltage |
| E_i | Total voltage to magnet |
| E_{0i} | Initial voltage to magnet |
| f, F | Nonlinear functions |
| F_{mag} | Magnetic force |
| g | Acceleration due to gravity |
| H | Magnetic field intensity |
| I_i | Current in coil |
| j | $\sqrt{-1}$ |
| k | Wave number |
| K | Feedback gain matrix |
| L | Inductance of circuit |
| L_i | Flux path length |
| M | Mass of rotor |
| n_1, n_2 | Real and imaginary parts of γ |
| N | Number of turns in coil |
| q | Complex wave number |
| R | Resistance of coil |
| s_i | Nondimensional velocity |
| t | Time |
| \vec{V} | Velocity vector |
| V | Velocity (magnitude) |
| W_d | Field energy density |
| W_f | Field energy stored |
| x | shaft displacement |
| X | State vector |
| y | shaft displacement |
| Z | Linearized state vector |
| α | System constant = $\mu_0 N^2 A$ |
| β | System constant = $L_1/\mu_{r1} + L_2/\mu_{r2}$ |
| γ | Complex number = $\cosh k\Delta + \mu_0 q/\mu k \sinh k\Delta$ |
| Γ | Magnetomotive force |
| δ | variation from equilibrium |
| Δ | Equilibrium gap length |
| θ | Magnet pole angle with respect to vertical |
| λ | Flux linkage |
| μ, μ_r | Permeability |
| σ | Electrical conductivity of rotor material |
| Σ | Closed surface, Summation sign |
| Φ | Magnetic flux |
| Ω | Spin speed of rotor |

FOUR MAGNET BEARING

The shaft is suspended within four magnets, as shown in Fig. 1. The shaft has high permeability and high conductivity and is not laminated. (Lamination would serve to inhibit eddy currents.) All of the four electromagnets are identical, modelled as a coil of N turns on a laminated core of high permeability. The coil has resistance R and an initial voltage E_0 applied. The dead weight is suspended by the difference in forces exerted by top and bottom magnets. All magnets carry a steady state voltage, adjusted so that at zero speed, the gap lengths under the magnets are equal.

This fully energized configuration was chosen so that the magnets could generate the effect of repulsion by decreasing the attraction. The horizontal magnets generate equal force when the shaft is centered and the control system is commanding equal voltages. The shaft displacement is measured by two coordinates (x, y) as shown in

Fig. 1, measured from the center of the clearance space in the horizontal and vertical directions respectively. When the rotor is not spinning, the center of the rotor is at the origin and the gap lengths are all equal to Δ .

If the shaft is not laminated, motion of the conducting shaft through the supporting magnetic fields will generate induced eddy currents. Eddy current effects cause both loss of lift and a drag force in the perpendicular direction. It is assumed that the rotor is spinning in the clockwise direction so that the drag force due to the top magnet acts in the negative x direction, that due to the right magnet acts in the y direction, and so on.

Several geometrical assumptions are made. The rotor always remains perfectly aligned within the bearing (no tilting). Under small displacements the surfaces of the rotor and the magnet pole faces are assumed to remain parallel. Since the individual poles are located at angles $\pm\theta$ relative to the vertical axis in the case of vertical magnets or relative to the horizontal axis in the case of horizontal magnets, it is assumed that when the rotor moves vertically a distance y , the change in gap length for the vertical magnets is $y\cos\theta$. Similarly, when the rotor moves horizontally by a distance x , the change in gap length for the horizontal magnets is $x\cos\theta$. Any other translational motion of the rotor can be written as a superposition of the motions in x and y directions. The effect of unequal gap lengths under a vertical magnet caused by a rotor motion in the horizontal direction or vice versa is neglected because the total gap length under that magnet remains constant.

The control system studied varies the voltage to each magnet in response to the motion of the mass. Such a suspension system with multiple magnets is a multiple input - multiple output system. A state variable feedback controller, designed on the basis of pole placement technique, is used to stabilize the system and meet the design specifications. Unlike in a single input - single output system, the multivariable problem has a much richer structure and has many gain matrices yielding the same pole placement [10]. The direct method of choosing an arbitrary vector and reducing the multi-input - multi - output system into a single input - single output system is used to obtain the gain matrix.

EQUATIONS OF MOTION

The differential equations of motion describing the response of the rotor are given by

$$\begin{aligned} M \ddot{y} &= \sum \vec{F}_{mag} \cdot \vec{n}_y - M g \\ M \ddot{x} &= \sum \vec{F}_{mag} \cdot \vec{n}_x \end{aligned} \quad (1)$$

where $\sum \vec{F}_{mag}$ are the vectorially combined magnetic forces from all the magnets. Expressions for resolutes of \vec{F}_{mag} have been derived in Appendix B for a single magnet. The reader is cautioned that the x, y coordinates in Appendix B are local tangential and normal directions for each individual magnet and do not correspond to the x, y coordinates for motion of the shaft. \vec{F}_{mag} includes the steady state attraction forces and eddy current forces (both repulsion and drag). Only spin velocity is assumed to generate eddy currents. Motion of the shaft (\dot{x}, \dot{y}) doesn't generate eddy currents.

The remaining differential equations are obtained from a voltage balance in each of the four electromagnetic circuits:

$$E_i = I_i R_i + N_i \phi_i \quad i = 1, 2, 3, 4 \quad (2)$$

where subscripts refer to the top, right, bottom, and left magnets respectively. An expression for the magnetic flux ϕ has been derived in Appendix B.

Expressions for the magnetic forces are given in Appendices A and B. If eddy currents are neglected, then there are no terms in the differential equations which depend on speed. In general

$$\vec{F}_{mag} = f(x, y, I_1, I_2, I_3, I_4, \Omega) \quad (3)$$

and

$$\phi_i = f(x, \dot{x}, y, \dot{y}, \dot{I}_1, \dot{I}_2, \dot{I}_3, \dot{I}_4, \Omega) \quad (4)$$

The general procedure is to

- (a) Determine E_{0i} such that the equilibrium location at zero speed is centered.
- (b) Design a state variable controller by pole placement.

- (c) Determine all steady state equilibrium locations as a function of speed.
(d) Linearize about equilibrium locations to determine stability as a function of speed.

Choosing eight state variables $\dot{y}, y, \dot{x}, x, I_1, I_2, I_3,$ and I_4 , Eqs. (1) and (2) can be put into a standard first order form

$$\dot{\mathbf{X}} = f(\mathbf{X}, \mathbf{E}, \Omega) \quad (5)$$

$$\mathbf{E} = \mathbf{E}_0 + \delta\mathbf{E} \quad (6)$$

$$\delta\mathbf{E} = K\mathbf{X} \quad (7)$$

$$\delta\mathbf{E} = (\delta E_1 \quad \delta E_2 \quad \delta E_3 \quad \delta E_4)^T \quad (8)$$

$$\mathbf{X} = (\dot{y} \quad y \quad \dot{x} \quad x \quad I_1 \quad I_2 \quad I_3 \quad I_4)^T \quad (9)$$

where \mathbf{X} is a 8-vector containing the state variables.

SINGLE MAGNET CASE

The single magnet suspension serves as a paradigm for the more complicated models which follow. Consider only the top magnet, with x constrained to be zero, and with no rotation ($\Omega = 0.0$). The approximation for \vec{F}_{mag} from Appendix A can be used, giving $\vec{F}_{mag} \propto (I^2, \frac{1}{h^2})$. Furthermore, \vec{F}_{mag} is always positive.

This system is well known to be unstable without feedback. A complete state variable feedback would be

$$\delta\mathbf{E} = [C_1 \quad C_2 \quad C_3] \begin{Bmatrix} x - x_0 \\ \dot{x} \\ I - I_0 \end{Bmatrix} \quad (10)$$

Fig. 2 shows how the static magnetic force is affected by the choice of C_1 . Obviously, there is some minimum value of C_1 to produce a positive slope at $x_0 = 0.001$. High values of C_1 produce a stiffer system but with a penalty. A second (unstable) equilibrium point exists. Increasing C_1 moves this point closer to the stable operating location. The safe operating domain in the state space is therefore decreased.

In addition, Fig. 2.5 shows the extreme nonlinearity of the system. The complete equations of motion can be written as a variation about the equilibrium point $(x_0, 0, I_0)$

$$\begin{aligned} u &= x - x_0 \\ v &= \dot{x} \\ w &= I - I_0 \end{aligned} \quad (11)$$

$$\frac{d}{dt} \begin{pmatrix} u \\ v \\ w \end{pmatrix} = [A] \begin{pmatrix} u \\ v \\ w \end{pmatrix} + [B] \delta\mathbf{E} \quad (12)$$

where

$$A = \begin{bmatrix} 0 & 1 & 0 \\ \frac{4gR}{E_0} \sqrt{\frac{M_g}{\alpha}} & 0 & -\frac{2gR}{E_0} \\ 0 & 2\sqrt{\frac{M_g}{\alpha}} & -\frac{E_0}{\alpha} \sqrt{\frac{\alpha}{M_g}} \end{bmatrix} \quad \text{and} \quad B = \begin{pmatrix} 0 \\ 0 \\ \frac{E_0}{\alpha R} \sqrt{\frac{\alpha}{M_g}} \end{pmatrix} \quad (13)$$

$$\delta\mathbf{E} = [C_1 \quad C_2 \quad C_3] \begin{pmatrix} u \\ v \\ w \end{pmatrix} \quad (14)$$

where

$$\alpha = \mu_0 N^2 A \quad (15)$$

Note, the equilibrium values (x_0, I_0, E_0) are related and consistent values must be used so that the position is actually a fixed point.

$$x_0 = \frac{1}{2} \left[\frac{E_0}{R} \sqrt{\frac{\alpha}{\mu_g}} - \beta \right] \quad (16)$$

$$I_0 = \frac{E_0}{R} \quad (17)$$

The various terms in Eq (13) can be identified as representing the magnetic force, the voltage drop due to back emf and the voltage drop due to inductance.

The controllability of this system can be determined from the rank of the controllability matrix Q .

$$Q = [B \quad AB \quad A^2B] \quad (18)$$

Substituting from Eq. (13) results in a matrix that has full rank. The total dynamic matrix turns out to be

$$\frac{d}{dt} \begin{pmatrix} u \\ v \\ w \end{pmatrix} = \begin{bmatrix} 0 & 1 & 0 \\ \frac{4gR}{E_0} \sqrt{\frac{Mg}{\alpha}} & 0 & -\frac{2gR}{E_0} \\ \frac{E_0}{\alpha R} \sqrt{\frac{\alpha}{Mg}} C_1 & 2\sqrt{\frac{Mg}{\alpha}} + \frac{E_0}{\alpha R} \sqrt{\frac{\alpha}{Mg}} C_2 & -\frac{E_0}{\alpha} \sqrt{\frac{\alpha}{Mg}} + \frac{E_0}{\alpha R} \sqrt{\frac{\alpha}{Mg}} C_3 \end{bmatrix} \begin{pmatrix} u \\ v \\ w \end{pmatrix} \quad (19)$$

The system is stable if

$$\begin{aligned} C_3 &< R \\ C_1 &> 2R \frac{\overline{Mg}}{\alpha} \left(1 - \frac{C_3}{R}\right) \\ C_1 &< 2R \frac{\overline{Mg}}{\alpha} \left(1 - \frac{C_3}{R}\right) + \frac{E_0}{\alpha} \sqrt{\frac{\alpha}{Mg}} \left(1 - \frac{C_3}{R}\right) C_2 \end{aligned}$$

The first constraint can be interpreted as requiring the coil to behave with positive resistance. The minimum value of C_1 is that required to overcome the effective negative stiffness of the magnetic force. The third condition enforces an upper bound on C_1 which is dependent on C_2 . This implies that the system cannot be stable without some velocity feedback. Apparently, the damping induced by the back emf is cancelled by the inductive lag of the coil, leaving an unstable system unless velocity feedback is used to add dissipation.

Given values of C_1, C_2, C_3 , the system may be linearized about the other equilibrium point (the one at lower gap). This point is found still to be unstable. Fig. 3 shows a sketch of the response in 3-D state space. The stabilized equilibrium point is a focus in two dimensions and has a stable subspace in the other dimension. The unstable equilibrium point is a saddle point in two dimensions and has a stable subspace in the third dimension. The presence of the unstable equilibrium point close to the stable one significantly affects the domain of convergence.

Rather than developing this problem further (including for example, the effect of eddy currents) discussion will be shifted to a two magnet configuration.

TWO MAGNET VERTICAL CASE

Consider a bearing consisting of only the top and bottom magnets in Fig. 1, with x constrained to be zero. This problem will study how the eddy currents affect the system, and so Appendix B will be used to represent the magnetic forces. The rotor is suspended by the difference in magnetic forces due to the top and bottom magnets. The stationary steady state voltages are such that the gaps are equal top and bottom, and the magnetic flux density is well below the saturation value of 1.5 - 2.0 webers/m².

The 8 state vector reduces to (y, y, I_1, I_3) . $\Sigma \vec{F}_{mag}$ becomes $F_{mag1} - F_{mag3}$. Since the system is constrained in x , the drag force due to eddy currents and the resulting coupling is neglected. The governing differential equations are

$$\begin{aligned} \frac{d}{dt} y &= \dot{y} \\ \frac{d}{dt} \dot{y} &= \frac{F_{mag1} - F_{mag3}}{M} - g \\ \frac{d}{dt} I_1 &= \frac{2(\Delta - y \cos \theta_1) + \beta_1}{\alpha_1} (E_{01} + \delta E_1 - R_1 I_1) - \frac{2y I_1 \cos \theta_1}{2(\Delta - y \cos \theta_1) + \beta_1} \\ \frac{d}{dt} I_3 &= \frac{2(\Delta - y \cos \theta_3) + \beta_3}{\alpha_3} (E_{03} + \delta E_3 - R_3 I_3) - \frac{2y I_3 \cos \theta_3}{2(\Delta - y \cos \theta_3) + \beta_3} \end{aligned} \quad (21)$$

The voltages E_{01}, E_{02} have been adjusted so that the equilibrium point is $y = 0$ with no spin speed. It then follows that

$$\begin{aligned} I_{01} &= \frac{E_{01}}{R_1} \\ I_{03} &= \frac{E_{03}}{R_3} \end{aligned} \quad (22)$$

$$Mg = F_{mag1} - F_{mag3}$$

A state variable feedback controller is designed for this case using the linearized set of equations at zero speed ($\Omega = 0.0$). Because eddy currents are not a factor at zero speed, the formulae in Appendix A can be used (giving a significant simplification over Appendix B). The linearized system can be written as

$$\dot{Z} = AZ + B \begin{pmatrix} \delta E_1 \\ \delta E_3 \end{pmatrix} \quad (23)$$

A is the Jacobian, B is the control matrix containing the inverse of the inductances of the two circuits at equilibrium and $(\delta E_1 \delta E_3)^T$ is the control vector for the perturbation voltages to the magnets.

This is a two input - single output system and unlike the previous single magnet case, there are many gain matrices K yielding the same eigenvalues. The solution to this control problem is discussed in [18]. However, the result is a gain matrix K such that the poles of the closed loop system (at zero speed) are placed at $-1000, -1000, -100 \pm j100$.

$$\begin{pmatrix} \delta E_1 \\ \delta E_3 \end{pmatrix} = K \begin{pmatrix} \dot{y} \\ y \\ \delta I_1 \\ \delta I_3 \end{pmatrix} \quad (24)$$

The complete closed loop system can now be considered with speed as a parameter. The equilibrium points are found by the numerical solution of the right hand side of Eq. (21) with ($\dot{y} = 0$). It turns out that there are 3 equilibrium points. This can be understood from a graph of the net magnetic force versus y as in Fig. 4. The point at $y = 0$ is a stable equilibrium point. However, points at $y \sim 4.4 \cdot 10^{-4}$ and $y \sim -8.4 \cdot 10^{-4}$ are also equilibrium points.

Furthermore, as speed increases, the force curve changes. The central equilibrium point drifts downwards, and the slope there decreases. Eventually, at sufficiently high speed, the central and lower equilibrium points coalesce and disappear. This is shown in Fig. 5.

The catastrophe occurs at $\Omega = 47000$ rpm for the values of parameters in this paper.

However, before that occurs, a more interesting dynamic phenomenon is observed. The dynamic equations can be linearized at each (shifting) equilibrium point. Since the equilibrium points must be found numerically, the linearization was also performed numerically using a central difference scheme in each state variable. The eigenvalues of the resulting dynamic matrix are shown in Fig. 6 as a function of the shaft speed Ω .

At zero speed, the eigenvalues are very near the design points $-1000, -1000, -100 \pm j100$. The difference is because magnetic circuit theory (Appendix A) is used in the zero speed controller design, but the full eddy current field theory solution (Appendix B) is used when linearizing and calculating eigenvalues. The system is stable (in a small neighborhood of the central equilibrium point) up to a value of $\Omega = 40406$ rpm, at which time a Hopf bifurcation (flutter instability) occurs.

The system loses stability through a single pair of eigenvalues crossing the imaginary axis at $\Omega = 40406$ rpm. In such a case, a limit cycle must grow from the bifurcation point. This can be either a stable limit cycle which increases in amplitude for $\Omega \geq 40406$ rpm or an unstable limit cycle which closes down around the focus as $\Omega \rightarrow 40406$ rpm. A standard bifurcation analysis was performed using the program BIFOR2 [19]. A stable supercritical limit cycle is predicted. The amplitude is shown in Fig. 7 along with the limit cycle actually found by simulation. It should be noted that the actual phase space is four dimensional and only a 2-D subspace is shown.

The reader is cautioned that the study was not extended to determine what (if anything) happens to the limit cycle when the two equilibrium points coalesce and disappear at 47000 rpm.

FOUR MAGNET CASE

Each coil is excited by initial constant voltages denoted by E_{oi} , $i = 1,2,3,4$, and the steady state magnetic forces (at $\Omega = 0$) are such that

$$\sum \vec{F}_{mag} = -mg\hat{y}. \quad (25)$$

The equilibrium points for this system at any spinning speed can be determined by equating the right hand side of Eqs. (5) to zero. That is,

$$0 = f(\mathbf{X}_{eq}, \Omega) \quad (26)$$

give the equilibrium points of the system. Eq. (26) represents a set of coupled nonlinear algebraic equations which has to be solved by a numerical technique. But, at zero speed, the equations decouple in x and y giving two separate problems, one of which has been discussed briefly. Without feedback control, this system has a single equilibrium point. It is possible to track the movement of this equilibrium point as speed increases [18].

To find the nature of the equilibrium point at any speed Ω , the differential equations are linearized and studied for their behavior in the neighborhood of the equilibrium point. As expected, the eigenvalues of the linearized system show that the four magnet bearing without active controls is inherently unstable.

A state variable feedback controller is added to the system to stabilize the bearing and provide it with suitable damping and dynamic characteristics. The effect of a gain matrix which is speed dependent is beyond the scope of this paper, and the control system is designed using the system characteristics at $\Omega = 0.0$. At zero speed, the equations of motion are uncoupled, and two 4th order control problems can be solved rather than one 8th order problem. State variable feedback controllers were designed for each subsystem to place the closed loop poles at -1000, -1000, $-100 \pm j100$. This placement provides dominantly second order response over a frequency range of 0 to 5000 rpm.

Note that because the system decouples, all states are not fed back to the control inputs for each magnet. For example, the variations of the gap length, velocity, and currents of the horizontal magnets are not being fed back to the vertical magnets and vice versa. Another advantage is that designing a state variable feedback controller for a four-input two-output system is more involved in terms of computation than two versions of a two-input single-output system. The feedback gain matrix K for this four magnet bearing is given in Table 3.

where

$$\begin{bmatrix} \delta E_1 \\ \delta E_2 \\ \delta E_3 \\ \delta E_4 \end{bmatrix} = [K] \mathbf{X} \quad (27)$$

It is not possible to derive analytical expressions for the equilibrium points of the system. However, the pattern of 3 equilibrium points for a pair of magnets in one dimension is extrapolated to an expectation of 3^2 equilibrium points in 2 dimensions. This has been confirmed by numerically solving the equations. As in the simpler cases, in designing the control system, the choice of pole assignments for the central equilibrium point (and resulting feedback gains and stiffness) affects the location of the surrounding equilibrium points. A faster, stiffer system (poles further into the left half of the s -plane) pulls the outlying equilibrium points closer together, as shown in Fig. (8).

As the spin speed increases, the equilibrium points shift due to changes in the magnetic forces, and in this case including the coupling due to eddy current drag forces. Furthermore, because the dynamics are affected by the gap lengths, the dynamic coefficients have changed, and the stability of the system is affected. Fig. 9 shows how all 9 points move within the clearance space. At low speeds not much happens but above 10,000 rpm the points begin to shift. At about 15,000 rpm points 3 and 9 coalesce and disappear.

At any running speed, the system can be linearized about any of the equilibrium points. Since the equations are rather unmanageable, the linearization was performed using a central difference method to find the derivatives of each function with respect to each state variable. The result is

$$\dot{\mathbf{Z}} = \mathbf{A} \mathbf{Z}. \quad (28)$$

where the \mathbf{Z} column vector contains perturbations about the speed dependent steady-state vector \mathbf{X} . Eigenvalues of \mathbf{A} give stability information about each point. Points 2-9 (the outlying points) were always unstable.

The eigenvalues corresponding to the central equilibrium point (1) as a function of the spinning speed are plotted in Fig. 10. The system is stable in a small neighborhood around the equilibrium point up to about 9306 rpm. As the spinning speed is further increased, a pair of complex conjugate eigenvalues crosses the imaginary axis with all the other eigenvalues still in the left half of the complex eigenvalue plane. This means that the system undergoes a classical Hopf bifurcation to flutter instability at the critical speed of 9306 rpm.

Because of the existence of the outlying unstable equilibrium points, a supercritical limit cycle was expected. However, a conventional Hopf bifurcation analysis on the full set of nonlinear equations, using BIFOR2, indicated that an unstable limit cycle will enclose the central equilibrium point for speeds less than Ω_{cr} . Fig. 11 shows three

transient responses at $\Omega = 2500$ rpm, calculated by numerical integration of the complete set of nonlinear equations. Two converge to the equilibrium point and one diverges. The domain of convergence was approximated by slowly incrementing $x(0)$ and $y(0)$ and noting convergence or divergence. The domain of convergence is marked in Figs. 11,12. This is an overly simple approach because changes in the initial conditions of the remaining 6 state variables are not explored. However, it does lend credence to the prediction of an enclosing unstable limit cycle.

Forced response of this system is discussed in detail in [18]. The global response is quite different from what might be expected from a linear analysis. The linear eigenvalues at $\Omega = 2500$ rpm indicates a damping ratio of 0.7. However, the orbit resulting from a periodic excitation of 25N only converges quite slowly (damping ratio ≤ 0.05). Further discussion is beyond the scope of this paper. The topic is opened here only to point out the pitfalls in extrapolating a linearized analysis.

CONCLUSION

Without considering eddy current effect, there is no speed dependent term in the constitutive model for a magnetic bearing. Eddy current cause a loss of effective lift which, viewed as an external load, causes a classical sag for a proportional controller. More importantly, eddy current drag causes coupling between (x, y) . Any change in the x gap affects the drag force in the y direction. Straightforward proportional control produces extra equilibrium points as the applied voltage is driven negative but the force remains attractive. These points are unstable but affect the global response of the system. In fact, designing a stiff system draws these points quite close to the equilibrium point. The equilibrium point is surrounded by an unstable limit cycle. Furthermore, as speed increases, the unstable limit cycle shrinks until the central point loses stability in a classical Hopf bifurcation. Above critical velocity, there is no equilibrium response.

The loss of lift is about 30% at 12500 rpm, which agrees approximately with experimental results of Yamamura [20]. The expression for the drag force under a single sinusoidal field density wave is the same as that obtained by Meisenholder [1].

The system may also lose stability by a simple catastrophe, the coalescing and joint annihilation of two equilibrium points. For the parameters used in this paper, this happens after the Hopf bifurcation. However, further parameter studies are needed to determine if this might occur before the Hopf bifurcation.

Further study is needed in designing state variable controllers. The zero speed design point is useful because it decouples the system, reducing the order. However, many other types of control can be envisioned.

The size of the enclosing unstable orbit is quite small, as shown in Fig. 12. A transient excitation could rather easily throw the shaft outside this into an unstable response. Also, a periodic excitation such as rotating unbalance, produces an orbit about the central equilibrium point. Simulation has indicated that if this orbit is large enough to touch or exceed the enclosing unstable limit cycle, the system becomes unstable. The loss of stability is quite complicated, with bifurcations of the periodic orbit and possibly bifurcation to chaos. Discussion of this is beyond the scope of this paper.

Further problems which should be investigated are the effects of flux saturation in the magnetic material. Also, the model developed in Appendix B is applicable to repulsion type electromagnets, which would run at high speed and likely require superconductivity to implement. Stability of these bearings has not yet been addressed.

A final comment is the topic of bearing coefficients (equivalent stiffness and damping matrices). The situation is different from that of journal bearings, it is not possible to determine the 8 classical coefficients just by differentiating the force expressions with respect to x, y, \dot{x}, \dot{y} . The dynamics of the electrical components must also be incorporated. However, in all cases, the response in one 'mode' was very fast(Fig. 3) indicating that some subspace reduction might be possible.

APPENDIX A ESTIMATION OF MAGNETIC LIFT FORCE

Magnetic circuit theory can be used to approximate the magnetic lift force of a single magnet, but eddy currents must be neglected. The following assumptions are made in deriving the expressions for the magnetic lift force:

1. Field fringing is neglected.
2. Magnetization curve is linear ($B = \mu H$).
3. Magnetic flux density B and field intensity H are uniform over cross-sections of the core, gap, or mass.

An electromagnetic circuit is considered whose elements are gap, core, and suspended mass, as shown in Fig. A.1. Each element has constant cross-section A_i and length L_i . The magnetic flux ϕ is assumed constant throughout the circuit, and Γ is the total magnetomotive force within the circuit elements.

The density relationship $\phi = BA$ and the constitutive law $B = \mu H$ can be used to express field intensity in the ferromagnetic material in terms of the field intensity within the air gap.

By definition $\Gamma = \int H dl$. Integrating around the circuit and equating Γ to the current linked (NI) results in an equation for field intensity within the air gap. The field energy is determined within each element $w = \frac{1}{2}\mu H^2$ and the total field energy is obtained by a volume integral over all the elements.

By definition, the force is the rate of change of stored field energy with respect to the mechanical displacement.

$$F_{mag} = \frac{\mu_0 N^2 A I^2}{(2x + \frac{L_1}{\mu_{r1}} + \frac{L_2}{\mu_{r2}})^2} \quad (A.1)$$

In addition, the total flux ϕ , the magnetic field density B , the magnetic flux linkage λ , and the inductance L can be expressed in terms of the gap length x and current I as:

$$\phi = \frac{\mu_0 N I A}{(2x + \frac{L_1}{\mu_{r1}} + \frac{L_2}{\mu_{r2}})} \quad (A.2)$$

$$B = \frac{\mu_0 N I}{(2x + \frac{L_1}{\mu_{r1}} + \frac{L_2}{\mu_{r2}})} \quad (A.3)$$

$$\lambda = \frac{\mu_0 N^2 I A}{(2x + \frac{L_1}{\mu_{r1}} + \frac{L_2}{\mu_{r2}})} \quad (A.4)$$

$$L = \frac{\mu_0 N^2 A}{(2x + \frac{L_1}{\mu_{r1}} + \frac{L_2}{\mu_{r2}})} \quad (A.5)$$

APPENDIX B ESTIMATION OF MAGNETIC FORCES INCLUDING EDDY CURRENT EFFECTS

Motion of a conducting material through a magnetic field will cause eddy currents to be generated within the material. These eddy currents will produce an additional magnetic field and change the net force acting across the air gap. The complete eddy current analysis for 4 magnets as shown in Fig. 1 is analytically intractable. (It is probably amenable to finite element techniques.) An approximate solution is developed in Ref [18], and only the assumptions, general method, and results will be presented here.

As the shaft starts spinning, the eddy currents tend to repel the applied magnetic field and the skin depth of penetration becomes very small. This motivates a semi infinite assumption in the radial direction.

First, the problem will be unwrapped and considered as periodic on a half-space. However, before net forces are calculated, the surface tractions predicted by Maxwell's stress tensor will be wrapped around a circular shaft.

Second, each magnet will be considered separately, and the magnetic field for each magnet can be determined individually. The net force of each magnet is then determined, leading to 4 vector forces which are then summed vectorially. An alternative (more complex) solution is developed in Ref. [18] to find net magnetic field for all four magnets as a single system (simultaneously). The net magnetic field of all 4 magnets may be determined, and a single force predicted. However, this approach requires the assumption that all the gaps are equal. At low spinning speeds there is no difference between the two methods. Only at very high speeds do the two differ. (For parameters in this paper, 4% at 10^5 rpm). The simpler technique has been used here.

The square wave applied flux density is expanded as a Fourier series

$$B(x) = \sum_i \frac{2B_o}{\pi i} \left[\cos\left(\frac{2bi}{D}\right) - \cos\left(\frac{2ai}{D}\right) \right] \sin\left(\frac{2ix}{D}\right) \quad (B.1)$$

or

$$B(x) = \sum_i B_i \sin(k_i x) \quad (B.2)$$

The field density and current density distributions within the moving material solve a linear problem, and hence the principle of superposition can be invoked and each harmonic handled separately. After finding the field density

inside the whole region, the forces acting on the rotor can be determined by calculating the Maxwell's stress tensor and integrating it over the surface area.

The following assumptions are made to simplify the analysis:

1. The conductive plate is infinite in x, z and positive y directions.
2. The conductivity σ and permeability μ are constants.
3. The field problem is two dimensional.

The equation that describes the distribution of the magnetic field in the conducting medium is derived from Maxwell's field equations [7].

$$-\frac{1}{\mu\sigma}\nabla^2\vec{B} + \frac{\partial\vec{B}}{\partial t} = \nabla \times (\vec{V} \times \vec{B}) \quad (\text{B.3})$$

where $\vec{B} = B_x\vec{e}_1 + B_y\vec{e}_2$ (\vec{e}_1 and \vec{e}_2 being unit vectors in x and y directions respectively). The y component B_y is determined from the y component of (B.3) The remaining component B_x can be determined from the relation $\nabla \cdot \vec{B} = 0$. The magnetic field is driven by the applied magnetic field density, and so solutions with the same traveling wave dependence on (x, t) are assumed. That is, it is assumed that the flux density takes the form

$$\vec{B} = [B_x(y)\vec{e}_1 + B_y(y)\vec{e}_2]e^{j(kx - \omega t)} \quad (\text{B.4})$$

The solution form in the y -direction is $e^{\pm qy}$ where

$$q_i = k_i \sqrt{1 + js} = k_i \sqrt{1 + j \frac{\mu\sigma V}{k_i^2}} \quad (\text{B.5})$$

Eqn (B.5) can be used to predict the skin depth.

The solution domain is divided into two regions, denoted by subscripts 1 and 2 respectively:

Region (1), the air gap where $\sigma = 0 (0 \leq y \leq \Delta)$; and

Region (2), the moving conducting medium ($\Delta \leq y \leq \infty$).

The solutions within each region have two constants of integration, determined from the following 4 boundary conditions:

- (1) one is set to zero because the solution cannot grow as $y \rightarrow \infty$.
- (2) the applied flux density at $y = 0$
- (3) At the interface $y = \Delta$, the condition of conservation of flux $\nabla \cdot \vec{B} = 0$ is invoked. Using the divergence theorem, this leads to $B_{y1} = B_{y2}$.
- (4) at the interface, $\nabla \times \vec{H} = 0$. Using Stokes theorem, this leads to $H_{x1} = H_{x2}$.

Hence, the flux density distribution throughout both regions can be determined.

The forces acting on the conducting medium are calculated by Maxwell's stress tensor [8]. For magnetic problems with currents and no charges, the forces acting on a body are given by

$$F = \int_{\Sigma} \frac{1}{\mu} [\vec{B}\vec{B} \cdot \hat{n} - \frac{1}{2}\vec{B}^2\hat{n}]dA \quad (\text{B.6})$$

where Σ is any closed surface surrounding the body and not containing any other body and B is the value of the field on the closed surface., Choosing a closed surface Σ such that it extends from $-\infty$ to ∞ and includes only the conducting medium, the integration is carried out with $\hat{n} = -\hat{e}_2$.

The complete flux density distribution in the whole region of Fig. B.1 due to all the applied sinusoidal waves is determined by superposing the individual fields. Each component of the field (B_x, B_y) is an infinite series in sine or cosine terms. The value of the \vec{B} field at the interface, which is required for calculating the forces, is calculated by substituting $y = \Delta$ and letting $B_x = B_{x1}$ and $B_y = B_{y1}$. Substituting for B and evaluating the integrals, the forces per unit area acting on the material turn out to be

$$F_x = -\frac{1}{4\mu_0} \frac{\mu_0}{\mu} \sum \frac{B_i^2}{(n_{1i}^2 + n_{2i}^2)} \frac{s_i}{R e^{\sqrt{1 + js_i}}} \quad (\text{B.7})$$

$$F_y = -\frac{1}{4\mu_0} \sum \frac{B_i^2}{(n_{1i}^2 + n_{2i}^2)} \left[1 - \left(\frac{\mu_0}{\mu}\right)^2 \sqrt{1 + s_i^2} \right] \quad (\text{B.8})$$

where

$$s_i = \frac{\mu\sigma V}{k_i} \quad (\text{B.9})$$

and where n_1 and n_2 are the real and imaginary parts of γ_i .

$$\gamma_i = [\cosh(k_i\Delta) + \frac{\mu_0 q_i}{\mu k_i} \sinh(k_i\Delta)] \quad (\text{B.10})$$

Eqs. (B.7) and (B.8) are the expressions for the drag and lift force per unit area acting on the moving conducting medium. As expected, when the currents are not induced in the slab ($V=0$) ($S=0$), there is no drag force (F_x) and F_y is the magnetic attractive force. There is an optimum value of V at which the maximum force per unit area F_x is produced. The lift force decreases as V is increased, and at some value of V the force becomes zero, and at high values acts in the opposite direction (repulsion). At very high values of V , there is no drag because all the flux is excluded from the material and the repulsion force reaches an asymptotic value irrespective of the permeability of the material.

It is interesting to note that the integral and the summation are interchangeable in order. That is, the force for one component of the fourier series can be determined and then summed or, as in the preceding, the fields summed and the force determined. This is perhaps surprising because the problem is nonlinear, but the infinite series for B_x and B_y are made up of sine and cosine terms which are orthogonal to one another and all the cross terms drop out during integration over one period.

The total flux can also be calculated and compared with that predicted by magnetic circuit theory (Appendix A). The more detailed solution is about 8% lower, showing the effects of magnetic circuit assumptions (uniform field density and no leakage in air gap).

For the magnetic bearing, the forces acting on a rotating shaft are calculated by wrapping one period of the B field distribution back onto the circular shaft. Choosing a closed surface Σ on the circumference of the rotor and simplifying the integral in Eq. (B.6) give the forces acting on the rotor per unit width as

$$F_x = -\frac{1}{\mu_0} \int_{-\frac{\pi p}{2}}^{\frac{\pi p}{2}} B_x B_y \cos\left(\frac{2x}{D}\right) dx - \frac{1}{2\mu_0} \int_{-\frac{\pi p}{2}}^{\frac{\pi p}{2}} (B_y^2 - B_x^2) \sin\left(\frac{2x}{D}\right) dx \quad (\text{B.11})$$

$$F_y = -\frac{1}{\mu_0} \int_{-\frac{\pi p}{2}}^{\frac{\pi p}{2}} B_x B_y \sin\left(\frac{2x}{D}\right) dx - \frac{1}{2\mu_0} \int_{-\frac{\pi p}{2}}^{\frac{\pi p}{2}} (B_y^2 - B_x^2) \cos\left(\frac{2x}{D}\right) dx \quad (\text{B.12})$$

where

$$B_x = B_{x1}(y) \Big|_{y=\Delta} = \sum -\frac{1}{\gamma_i} \frac{\mu_0 q_i}{\mu k_i} B_i e^{j k_i x} \quad (\text{B.13})$$

$$B_y = B_{y1}(y) \Big|_{y=\Delta} = \sum \frac{1}{\gamma_i} \frac{q_i}{k_i} B_i e^{j k_i x} \quad (\text{B.14})$$

The effect on the values of the forces of the number of terms used in the fourier series was investigated. The magnetic forces were calculated at different spinning speeds using 10, 25, 50, 100, and 500 terms in the series. There is very little change in the results when the number of terms used in the series is 50 or more. There is approximately 3% change in the lift force when the number of terms is increased from 10 to 25 or from 25 to 50. The change is much less in the case of drag force calculations. Striking a compromise between these two, and to save computer time, 25 terms were used in all the calculations in this paper.

REFERENCES

1. Meisenholder, S.G.; Wang, T.C.: *Dynamic Analysis of an Electromagnetic Suspension System for a Suspended Vehicle System*, TRW Systems Group, Prepared for Federal Railroad Administration, 1972.
2. Wormley, D.N.; et al.: *Noncontacting Suspension and Propulsion for Ground Transportation*, University Research for U.S. Department of Transportation, December 1979.
3. Nikolajsen, J.L.; et al.: Investigation of an Electromagnetic Damper for Vibration Control of a Transmission Shaft, *Proc Inst Mech Engrs*, Vol 193, I Mech E, 1979.
4. Habermann, H.; Liard, G.L.: Practical Magnetic Bearings, *IEEE Spectrum*, pp 26-30, September 1979.
5. Habermann, H.; Liard, G.L.: An Active Magnetic Bearing System, *Tribology International*, pp 85-89, April 1980.
6. Bartlett, R.A.: *Active Vibration Control of Flexible Rotors using Magnetic Bearings*, M.S. Thesis, Cornell University, January 1984.
7. Kailath, T.: *Linear Systems*, Prentice Hall, Inc., 1980.
8. Geary, P.J.: Magnetic and Electric Suspension, *British Scientific Instrument Research Association Report R314*.
9. Frazier, R.H.; et. al.: *Magnetic and Electric Suspensions*, The MIT Press, 1974.
10. Kaplan, B.Z.: A New Analysis of Tuned Circuit Levitators *International Journal of Nonlinear Mechanics*, Vol 9, pp 75-87, Pergamon Press, 1974.
11. Studer, P.A.: A Practical Magnetic Bearing, *IEEE Transactions on Magnetics*, Vol MAG-13, n5, September 1977.
12. Moon, F.C.: *Magneto-solid Mechanics*, Cornell University, to be Published.
13. Woodson, H.H.; Melcher, J.R.: *Electromechanical Dynamics Part I, Part II*, John Wiley and Sons, Inc., New York, 1968.
14. Chari, M.V.K.; Silvester, P.P.: *Finite Elements in Electrical and Magnetic Field Problems*, John Wiley and Sons, Inc., New York, 1980.
15. Yoshimoto, T.: Eddy Current Effect in a Magnetic Bearing Model *IEEE Transactions on Magnetics*, Vol MAG-19, n5, September, 1983.
16. Wang, T.C.; et. al.: Single-Sided Linear Induction Motor, Sixth Annual IEEE-IGA Meeting, October, 1971.
17. Matsumara, F.; et. al.: Fundamental Equation for Horizontal Shaft Bearing and its Control System Design *Electrical Engineering in Japan*, Vol 101, n3, pp 123, May-June 1981.
18. K.V. Hebbale: *A Theoretical Model for the Study of Nonlinear Dynamics of Magnetic Bearings*, Ph.D. Dissertation, Cornell University, Jan., 1985.
19. Hassard, B.D.; et. al.: *Theory and Applications of Hopf Bifurcations*, London Mathematical Society Lecture and Notes 41, Cambridge University Press, 1981.
20. Yamamura, S.; Ito, T.: Analysis of Speed Characteristics of Attractive Magnet for Magnetic Levitation of Vehicles, *IEEE Transactions on Magnetics*, Vol MAG-11, n5, September, 1975.

TABLE 1
Single Magnet Suspension Parameters

| | |
|--|------------------------------|
| Mass M | = 8.91 kg |
| Acceleration due to gravity g | = 9.80665 m/sec ² |
| Area of cross section A | = 0.00025 m ² |
| Initial voltage E ₀ | = 5.0 volts |
| Resistance of coil R | = 3.0 ohms |
| Path length in core L ₁ | = 0.28 m |
| Path length in Mass L ₂ | = 0.05 m |
| Permeability of free space μ ₀ | = 4πE - 07H/m |
| Relative permeability of core material μ _{r1} | = 10000.0 |
| Relative permeability of mass material μ _{r2} | = 100.0 |
| Number of turns N | = 800 |

FEEDBACK GAIN MATRIX: Poles at -1000 , -100 ± j100

$$K = [261013.13 \ 1486.86 \ -92.44]$$

TABLE 2
Two Magnet Bearing Parameters

| | |
|---|------------------|
| ROTOR | |
| Diameter of rotor D | = 0.15 m |
| Mass of rotor M | = 15.6 kg |
| Path length in rotor L_2 | = 0.05 m |
| Relative permeability of mass material μ_{r2} | = 100.0 |
| Electrical conductivity of mass material σ | = 1.0 E+07 mho/m |
| MAGNET | |
| Pole angle | = 15 degrees |
| Path length in core L_1 | = 0.28 m |
| Relative permeability of core material μ_{r1} | = 10000.0 |
| Area of pole face A | = 0.00025 m^2 |
| Width of pole face W | = 0.008333 m |
| Number of turns N | = 800.0 |
| Distance of pole corner a | = 0.0075 m |
| Distance of pole corner b | = 0.0375 m |
| Initial voltage (top) E_{01} | = 7.5 volts |
| Initial voltage (right) E_{02} | = 2.5 volts |
| Initial voltage (bottom) E_{03} | = 2.5 volts |
| Initial voltage (left) E_{04} | = 2.5 volts |
| Resistance of coil R | = 3.0 ohms |

TWO MAGNET FEEDBACK GAIN MATRIX
Poles at -1000, -1000, -100 ± j100

$$K = \begin{bmatrix} 4570751.1 & 11052.9 & -565.5 & -2200.5 \\ 1523583.7 & 3684.3 & -188.5 & -733.5 \end{bmatrix}$$

TABLE 3
Feedback Gain Matrix for Four Magnet Bearing

$$K^T = \begin{bmatrix} 4570751.1 & 0.0 & 1523583.7 & 0.0 \\ 11052.9 & 0.0 & 3684.3 & 0.0 \\ 0.0 & 7185390.6 & 0.0 & 7185390.6 \\ 0.0 & 18021.2 & 0.0 & 18021.2 \\ -5675.5 & 0.0 & -188.5 & 0.0 \\ 0.0 & -3500.0 & 0.0 & -3500.0 \\ -2200.5 & 0.0 & -733.5 & 0.0 \\ 0.0 & -3677.7 & 0.0 & -3677.7 \end{bmatrix}$$

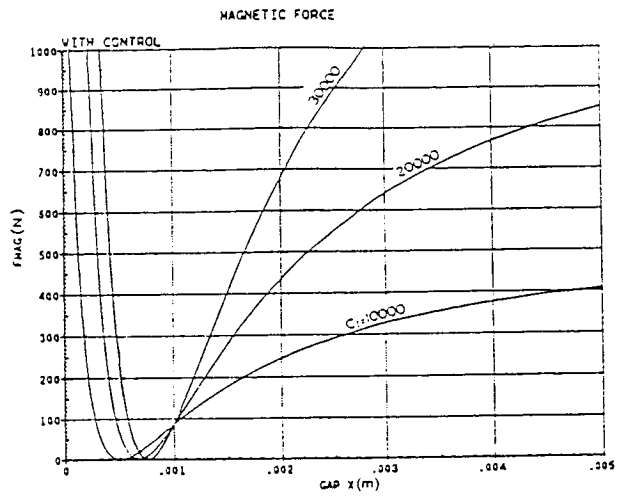


Figure 1: Four Magnet Bearing

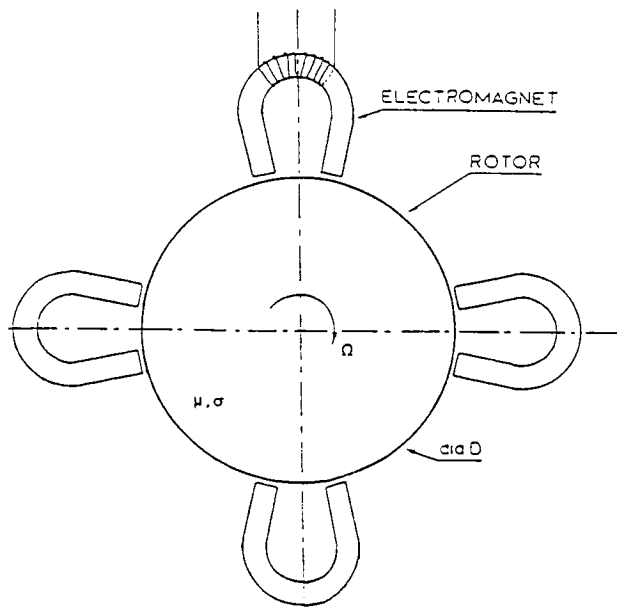


Figure 2: Effect of Feedback Gain on Stiffness of Single Magnet Suspension

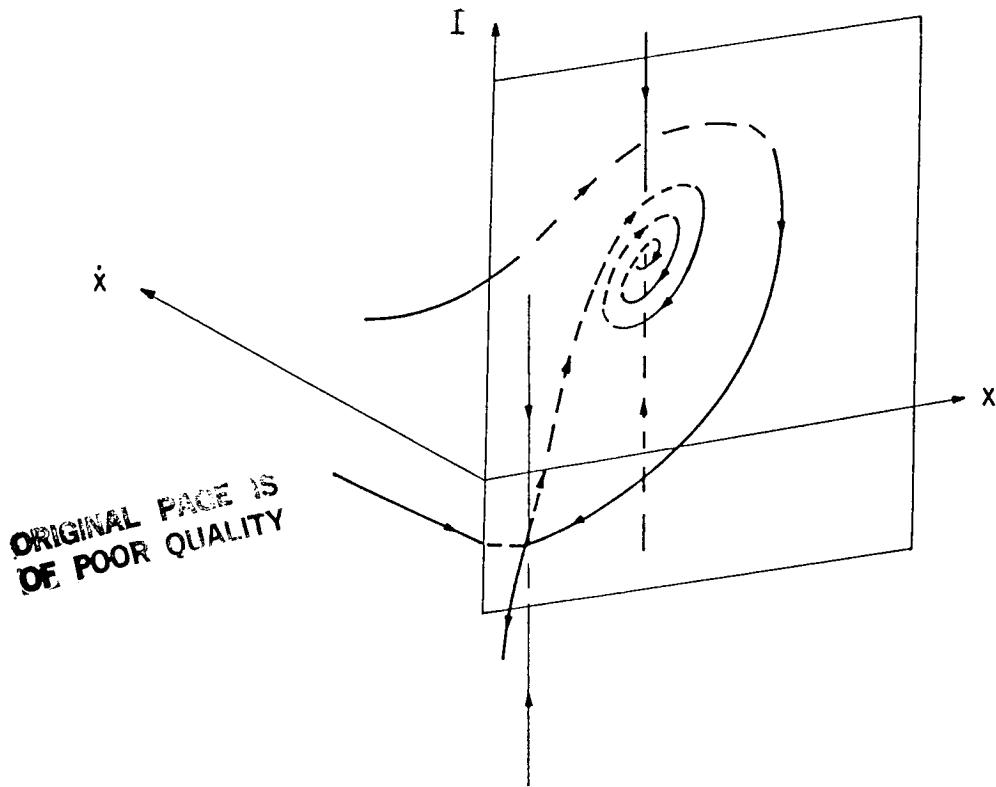


Figure 3: Global Stability of Single Magnet Suspension

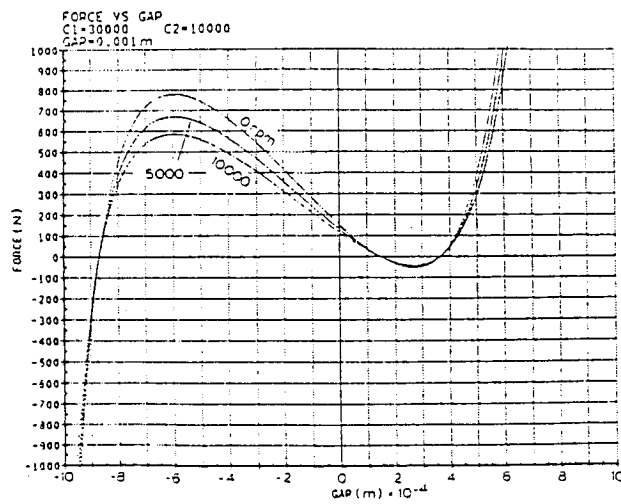


Figure 4: Net Magnetic Force vs Shaft Displacement, with Feedback

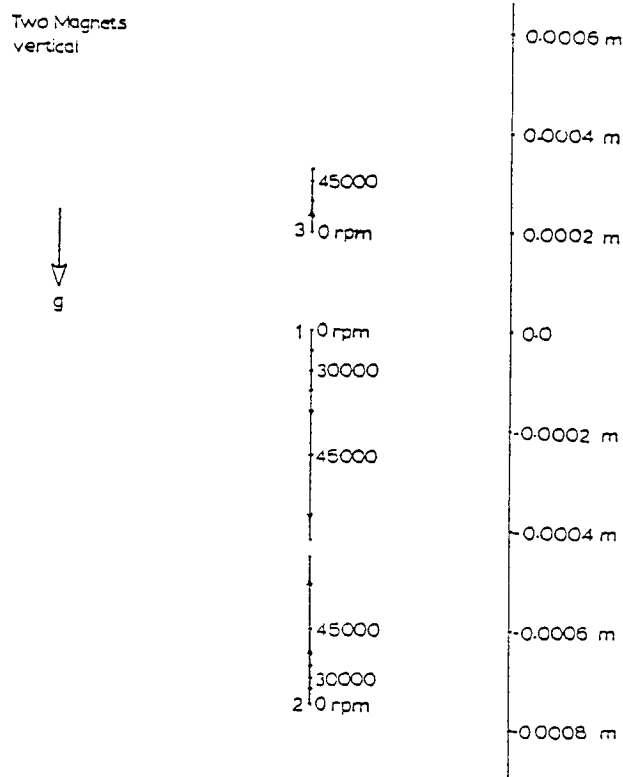


Figure 5: Locus of Equilibrium Points, with Feedback, as Speed Varies

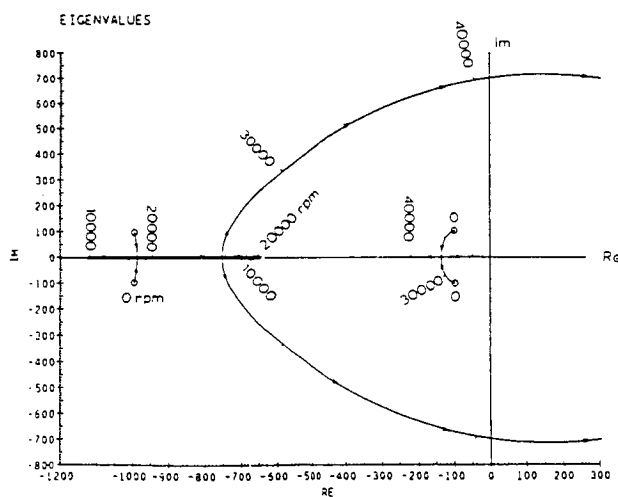


Figure 6: Root Locus for Two Magnet Bearing, as Speed Varies

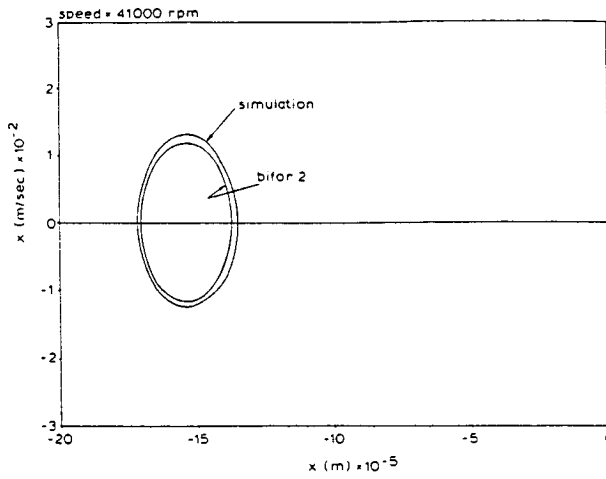


Figure 7: Limit Cycle Comparison for Two Magnet Bearing

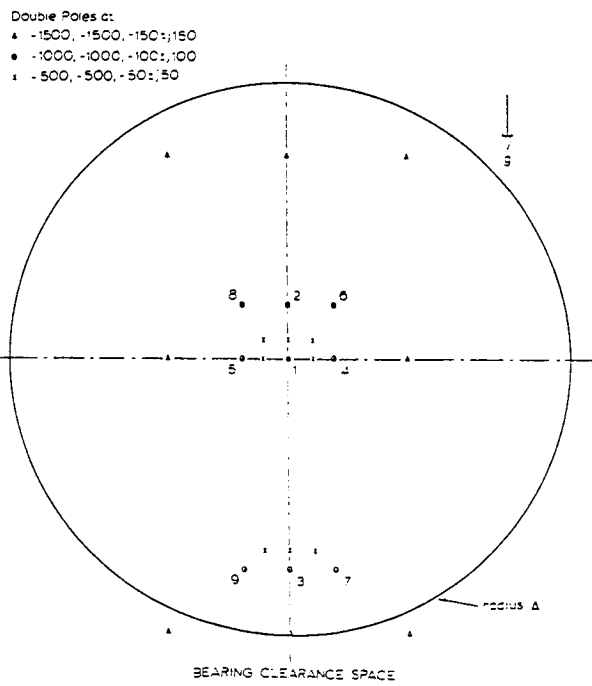


Figure 8: Equilibrium Points at $\Omega = 0$ for Three Different Pole Assignments

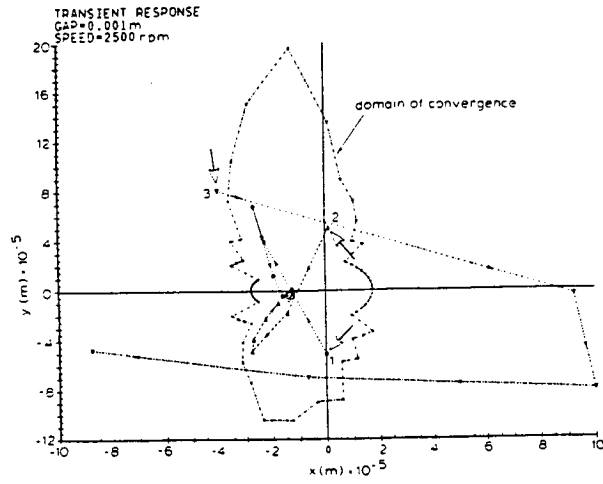


Figure 11: Transient Response at 2500 rpm

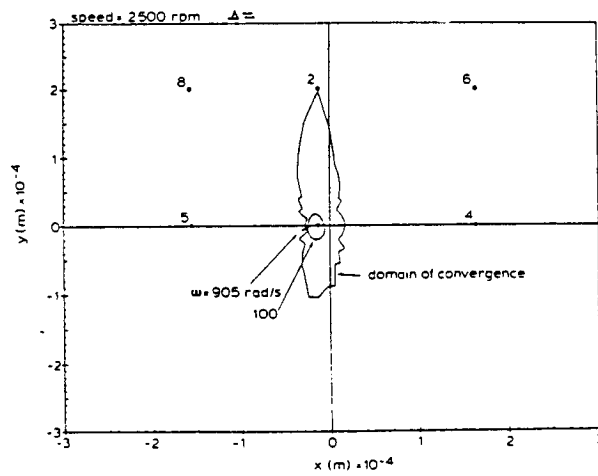


Figure 12: Equilibrium Points, Domain of Convergence, $\Delta = ?$

ORIGINAL PAGE IS
OF POOR QUALITY

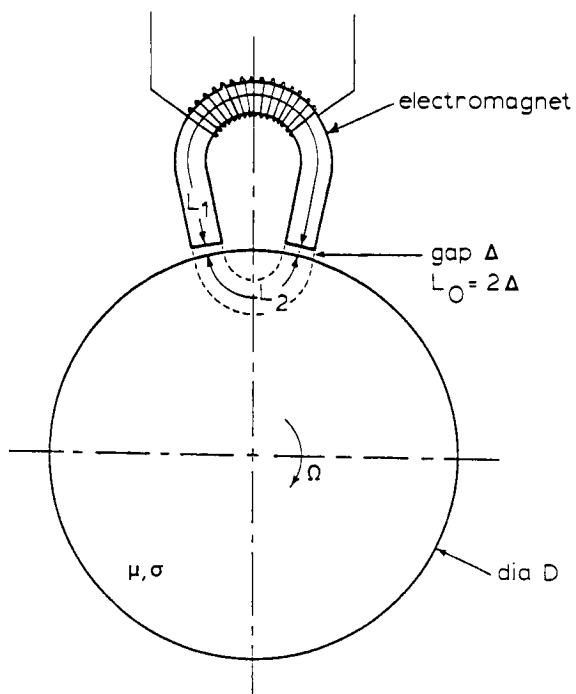


Figure A.1: Ferromagnetic Rotor under a Single Electromagnet

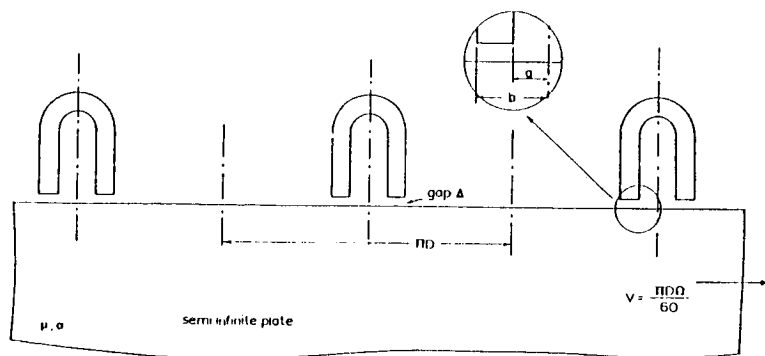


Figure B.1: Semi-Infinite Plane under a Series of Electromagnets

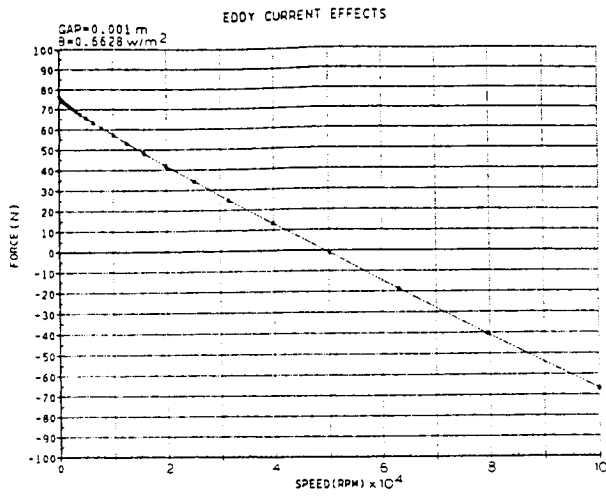


Figure B.2: Lift Force as a function of Spin Speed

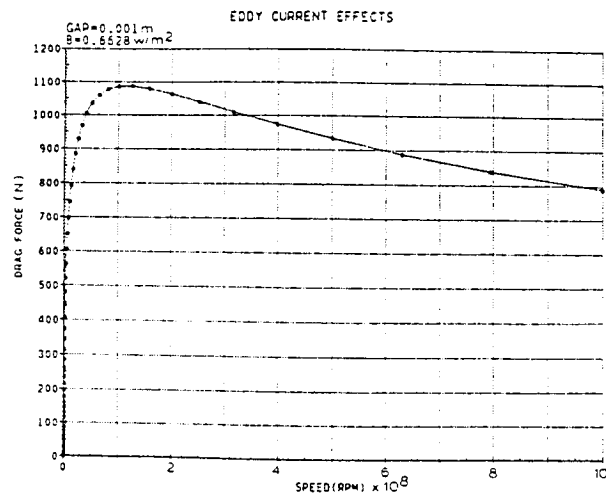


Figure B.3: Drag Force as a function of Spin Speed